Optics Letters

# Lensfree dynamic super-resolved phase imaging based on active micro-scanning

Jialin Zhang,[1,2,3] Qian Chen,[1,2,4] Jiaji Li,[1,2,3] Jiasong Sun,[1,2,3] and Chao Zuo[1,2,3,*]

[1]School of Electronic and Optical Engineering, Nanjing University of Science and Technology, No. 200 Xiaolingwei Street, Nanjing, Jiangsu Province 210094, China
[2]Jiangsu Key Laboratory of Spectral Imaging & Intelligent Sense, Nanjing, Jiangsu Province 210094, China
[3]Smart Computational Imaging Laboratory (SCILab), Nanjing University of Science and Technology, Nanjing, Jiangsu Province 210094, China
[4]e-mail: chenqian@njust.edu.cn
*Corresponding author: zuochao@njust.edu.cn

Received 29 March 2018; revised 17 June 2018; accepted 10 July 2018; posted 10 July 2018 (Doc. ID 327117); published 27 July 2018

**In this Letter, we present a new active micro-scanning-based imaging platform and associated super-resolution (SR) phase retrieval method in lensfree microscopy to achieve SR dynamic phase imaging. The samples are illuminated by a nearly coherent illumination system, where two orthogonal parallel plates are inserted into the light path and rotate to achieve controllable source micro-scanning, permitting sub-pixel shifts of the holograms on x- and y-axis directions independently. Then sequential low-resolution sub-pixel-shifted holograms are processed to enhance spatial resolution and reconstruct quantitative phase images of the sample simultaneously. The reconstruction result of the benchmark quantitative phase microscopy target (QPT$^{TM}$) demonstrates a half-pitch lateral resolution of 775 nm across a large field-of-view of ~29.84 mm$^2$, surpassing 2.15 times that of the theoretical Nyquist–Shannon sampling resolution limit imposed by the pixel size of the imaging sensor (1.67 μm). The proposed approach is also evaluated by imaging unstained HeLa cells, suggesting it is a promising toolset for high-throughput monitoring and quantitative analysis of unlabeled biological samples.** 

***OCIS codes:*** (100.5070) Phase retrieval; (100.6640) Superresolution; (110.1758) Computational imaging.

https://doi.org/10.1364/OL.43.003714

Lensfree on-chip microscopy is an emerging technique for point-of-care imaging and pathology applications, with the advantages of significantly larger field-of-view (FOV) and extremely compact optical system, especially when compared to its lens-based counterparts [1–3]. By placing the sample close to the active area of an image sensor, the FOV of the lensfree on-chip imaging platform is equal to the active area of the sensor chip. However, since the recorded holographic fringes are no longer magnified (unit magnification), the spatial aliasing resulting from the pixel size of the image sensor chip becomes the key limiting factor for achieving high imaging resolution [3–5]. This physical limit can be overcome (or at least alleviated) by pixel super-resolution (SR) techniques, in which the hologram with a smaller effective pixel size can be synthesized from multiple low-resolution (LR) measurements that are recorded at different sub-pixel displacements between the image sensor and the object plane [4–6]. To capture these sub-pixel shifted LR images, either the illumination source or the samples needs to be precisely displaced which, in turn, requires extra controllable mechanical devices with very high precision and repeatability. Alternatively, sub-pixels shifts can also be created by using a fiber-optic array as a programmable light source without involving any mechanic movement [7]. However, the fabrication of such a light source has remained complicated and challenging, requiring precise alignment of several micron-scale fibers within a small area. More recently, several more advanced pixel SR approaches have been proposed by utilizing different wavelengths [8], illumination angles [5,9], or sample-to-sensor distances [3,5]. All these implementations inevitably require high-precision tunable devices, complicate the mechanical design, and increase the overall costs of the system.

Apart from improving the imaging resolution, increasing the image contrast is also essential, especially when the specimen of interest is transparent. Such objects, including most unlabeled live cells and tissues, do not absorb or scatter visible light significantly and, thus, exhibit very low contrast under conventional bright-field microscopy. During recent years, quantitative phase imaging (QPI) [10,11] has emerged as an invaluable label-free imaging modality that offers advantages over conventional phase contrast [12] and differential interference contrast imaging [13] for quantitative analyses, such as measuring the optical thickness and refractive index of the imaged structure. However, conventional QPI approaches rely on intricate optical configurations, and it is always desirable to implement QPI on the simplified lensfree platform with minimal hardware requirements. Though some success has been demonstrated for spatial and temporal resolution enhancement in lensfree imaging of stained, absorbent, or relatively sparse samples [2,3,5,14], high-quality, low-noise SR phase imaging results of unlabeled biological samples have been rarely reported.

To address the above-mentioned two problems, in this Letter, a new active micro-scanning based lensfree microscopy

platform is presented based on controllable shifts of the light source. We also propose a unified computational framework for phase retrieval and resolution enhancement by exploiting the space-time information of an image sequence in a recursive manner, allowing for SR phase imaging of dynamic samples. As illustrated in Fig. 1, instead of directly moving the light source or the samples, we insert two parallel glass plates into the light path between the source and the imaging sensor. In our real system, two regular microscope slides (Citoglas, thickness 1 mm, dimension 75 × 25 $mm^2$) are rotated by two low-cost micro-servos (SG90, Tower Pro, ~$1), which are driven by an Arduino development board. A single-mode fiber-coupled light source (LP660-SF20, Thorlabs, wavelength $\lambda = 660$ nm) illuminates the sample through two plates and, finally, the diffraction patterns (in-line holograms) are captured by a monochrome camera (DMM 27UJ003-ML, the imaging source). The distance between the image plane and the samples $z_2$ is ~0.4–10 mm, and the light source is ~10–15 cm ($z_1$) above the samples.

In our system, the rotation axes of the two parallel plates are perpendicular to each other and normal to the optical axis ($z$) in order to produce the lateral shifts of the source in both $x$ and $y$ directions. In the beginning, both the two parallel plates are perpendicular to the optical axis, and the lateral shift $\delta_y$ in the $y$ direction will be generated when one plate rotates around the $x$ axis:

$$\delta_y = d \sin\theta\left(1 - \frac{\cos\theta}{\sqrt{n^2 - \sin^2\theta}}\right), \tag{1}$$

where $d$ is the thickness of the parallel plate, $n$ is the refractive index of the parallel plate, $\theta$ is the angle between the incident light and the normal direction of the parallel-plate plane. As the magnification of the entire system approaches 1 ($z_1 \gg z_2$), the large $z_1/z_2$ ratio enables wide-field lensfree holography. Simple geometrical optics approximations show that the object hologram at the detector plane can be sub-pixel shifted by translating the illumination source parallel to the detector plane [4]:

$$\varepsilon_y = \frac{z_2}{z_1} \times \frac{n_1}{n_2} \times \delta_y, \tag{2}$$

where $\varepsilon_y$ is the shift of the hologram corresponding to the shift of the light source $\delta_y$, $n_1$ is the refractive index of the air, and $n_2$ is the refractive index of the cover glass of the camera. Given typical experimental parameters ($n = 1.52$, $n_1 = 1$, $n_2 = 1.51$, $z_1 = 10$ cm, $z_2 = 0.5$ mm), an angular change by $-50° \sim +50°$ shifts the image by $-1.55 \sim 1.55$ μm, which is on the sub-pixel level. Therefore, a sub-pixel hologram shift can be realized with relatively large angle rotation, which can be achieved by the low-cost mechanical devices. Furthermore, the exact sub-pixel shifts are directly estimated from the captured LR holograms based on a cross-correlation-based sub-pixel registration algorithm [15], which makes our approach self-calibration and almost independent of the precision or accuracy of the micro-servo.

By changing the rotation angles of the two plates, a set of LR holograms $I^m_{\text{cap}}$ is obtained sequentially and repeatedly from a displacement matrix of varied shifts of the light source (5 × 5 different positions), where $m$ is the index of the captured images which is in chronological order. The following process (summarized in Fig. 2) will be implemented to overcome pixel aliasing and recover a pixel SR QPI sequence.

**Step 1: initial phase estimation.** Solving the transport of intensity equation (TIE) to obtain a phase estimate $\phi_{\text{TIE}}$ [16]. Note that by assuming a pure phase object, the in-focus intensity distribution is uniform (no need to capture), and the captured out-of-focus image $I^1_{\text{cap}}$ with the uniform intensity is sufficient to solve the TIE. Then the retrieved phase will be further refined by the iterative Gerchberg–Saxton (G-S) phase retrieval algorithm [17]. After five iterations, an initial guess of the phase distribution at the object plane can be generated.

**Step 2: object space constraint.** The up-sampled initial guess $U_{\text{ini}}$ at the object plane is updated based on the intensity constraint provided by the smoothed intensity distribution $I^m_0$ (which is again approximately uniform for a pure phase object [18] and estimated by low-pass filtering the defocused image $I^m_{\text{cap}}$ with a very large convolution kernel), and the resultant complex field $U^m_{\text{obj}}$ is propagated to the image plane to obtain the new complex amplitude $U^m_{\text{cam}}$ ($m \leftarrow m + 1$).

**Step 3: sub-pixel registration.** To directly estimate the exact sub-pixel shifts between the adjacent frames, the square modulus of $U^m_{\text{cam}}$ is registered with the reference intensity image $I^m_{\text{cap\_up}}$ based on the cross-correlation-based sub-pixel registration algorithm [15], where $I^m_{\text{cap\_up}}$ is the up-sampled version of $I^m_{\text{cap}}$. The aligned complex field after sub-pixel registration is denoted as $U^m_{\text{reg}}$ ($I^m_{\text{reg}} = |U^m_{\text{reg}}|^2$).

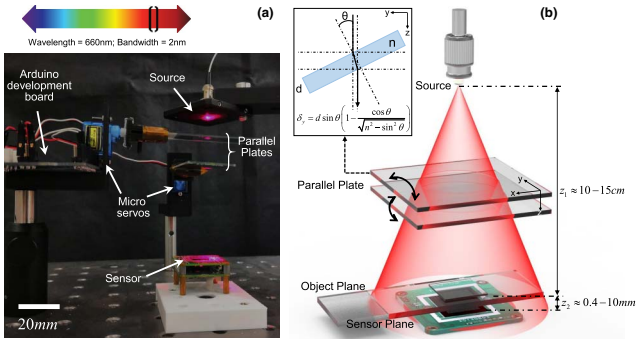


**Fig. 1.** Lensfree system setup based on active source microscanning. (a) Photograph of the setup used in our experiment. (b) Structure diagram of the optical setup. The range of the rotation angle is about $-50° \sim +50°$.

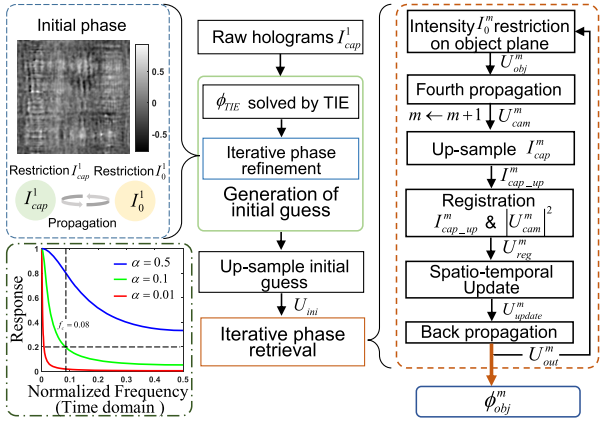


**Fig. 2.** Flow chart of the lensfree dynamic SR phase retrieval. The upper left is the generation of the initial guess, and the right is the process of iterative phase reconstruction. The lower left is the frequency response of **Step 5** with simplification.

**Step 4: image space constraint.** The intensity $I^m_{\text{reg}}$ is updated based on the intensity constraint imposed by the captured LR hologram: $I^m_{\text{update}} = \frac{I^m_{\text{cap\_up}}}{I^m_{\text{reg\_cal}}} \times I^m_{\text{reg}}$, where $I^m_{\text{reg\_cal}}$ is the value calculated by down-sampling $I^m_{\text{reg}}$ and then implementing up-sampling with the nearest neighborhood interpolation. This step guarantees that the updated intensity $I^m_{\text{update}}$ after pixel binning coincides with the captured LR intensity $I^m_{\text{cap}}$.

**Step 5: relaxed spatio-temporal update.** The complex amplitude $U^m_{\text{reg}}$ at the image plane is updated in a recursive manner: $U^m_{\text{update}} = (1-\alpha) \times U^m_{\text{reg}} + \alpha \times \sqrt{I^m_{\text{update}}} \cdot \exp(i \cdot \arg(U^m_{\text{reg}}))$, where $\arg(\cdot)$ is the function to obtain the argument. In fact, the updating process can be regarded as a temporal low-pass filter, where $\alpha$ is the relaxation factor (time constant) controlling the amount of feedback from the previous estimate of the algorithm. When $\alpha = 1$, as in conventional G-S phase retrieval, the phase estimate is fully constrained by the current intensity $I^m_{\text{cap}}$ and, thus, has no effect on resolution improvement. Using an $\alpha$ less than one allows the information from multiple sub-pixel shifted images to blend together, making it a spatio-temporal process. In this Letter, we choose $\alpha = 0.1$ to properly incorporate the information from ~25 LR images (frequency response >0.2, as shown in the inset of Fig. 2) to enhance the resolution while reducing the influence of noise.

**Step 6: phase reconstruction.** The updated complex amplitude $U^m_{\text{update}}$ is back-propagated to the object plane ($U^m_{\text{out}}$), and the SR phase information $\phi^m_{\text{obj}} = \arg(U^m_{\text{out}})$ corresponds to the moment at which the frame $I^m_{\text{cap}}$ can be recovered. For the next incoming captured image, the above outlined steps (**Steps 2** to **5**) are then executed iteratively with the $U^m_{\text{out}}$ taken as the initial value for the next iteration cycle.

To verify the resolution enhancement of the proposed approach quantitatively, we imaged a benchmark quantitative phase microscopy target (QPT$^{\text{TM}}$) with the micro-scanning setup. Figure 3(a) shows one raw intensity image, and Fig. 3(b) shows one zoom-in corresponding to the area outlined by the red rectangle. Since the sample is a pure phase object, it can hardly be observed under a normal bright field microscope, as shown in Fig. 3(c). Figures 3(d)–3(e) are the reconstructed phase images corresponding to the same raw captured image (e.g., No. 8 frame) based on the conventional G-S algorithm [17] and the proposed approach, respectively. Note that in the G-S algorithm, we employed the pure phase constraint and registered each input intensity during an image space update, but the pixel binning model and relaxation factor were not incorporated ($\alpha = 1$). As shown in Figs. 3(f)–3(h), the conventional G-S algorithm does not provide obvious resolution enhancement with a half-pitch resolution of 1.67 μm limited by the pixel size of the camera. When our approach was applied, obvious enhancement in image resolution and quality could be observed, with the half-pitch resolution improved from ~1.67 μm to 775 nm, as demonstrated in Figs. 3(g)–3(i). Not only the reconstructed resolution comparable with the Rayleigh resolution limit provided by a normal 10× 0.25 NA objective (half-pitch resolution 805 nm) is significantly improved, but the quantitative phase information of the sample can be recovered. Furthermore, in a lensfree microscope, the imaging FOV of ~29.84 mm$^2$ is approximately 100-fold that achieved by a traditional 10× lens-based microscope.

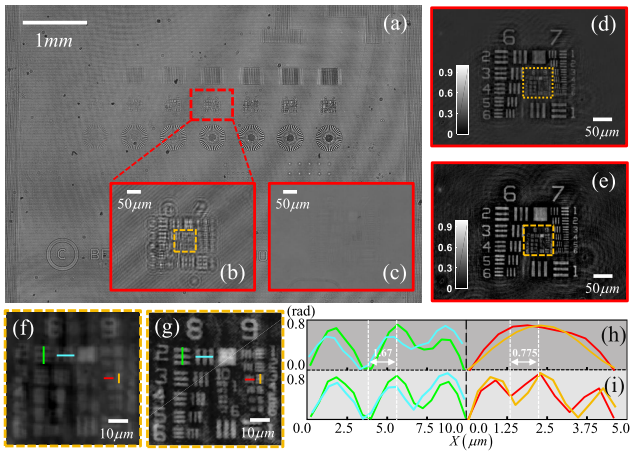


**Fig. 3.** Experimental results of the phase resolution target. (a) Raw image obtained in a single shot. (b) Enlargement of the boxed area in (a). (c) Full FOV image captured with an Olympus Plan 10× 0.25 NA objective lens. (d)–(e) Reconstructed results with the conventional G-S algorithm and the proposed algorithm, respectively. (f)–(g) Zoomed areas, respectively, selected by rectangles in (d)–(e). The FOV of (b)–(e) and (f)–(g) separately corresponds to the boxed area in (a) and (b). (h)–(i), respectively, show the phase values across sections in (f)–(g).

Experiments on unstained HeLa cells were performed to verify the applicability of the proposed method for imaging biological samples. The adherent HeLa cells are immersed and fixed in the buffered glycerol. Figure 4(a) shows the whole FOV image of HeLa cells slide, and Figs. 4(b1)–4(b3) are the reconstructed results based on a traditional G-S method, as mentioned before. Although the phases of the cells can be largely recovered, the results still suffer from low spatial resolution and large background noise. In contrast, due to the effect of spatio-temporal averaging and resolution enhancement, the proposed approach provides high-resolution, high-quality phase reconstruction with a much smoother background. Besides, the low-frequency component of the phase can be more accurately recovered because the initial guess of phase is recovered by the TIE, which provides better low-frequency

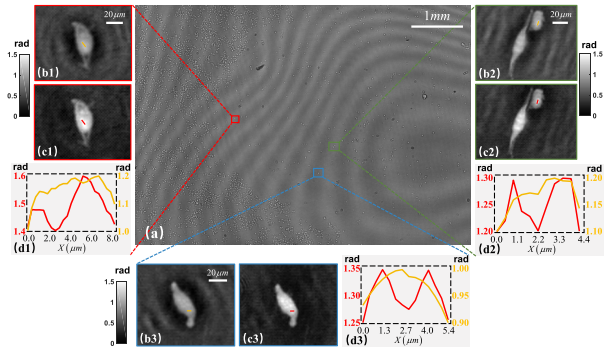


**Fig. 4.** Experimental results of fixed HeLa cells. (a) Full FOV image captured by the camera directly. (b1)–(b3) Reconstructed results of the respective boxed areas in (a) with the conventional G-S algorithm. (c1)–(c3) Reconstructed results correspond to the selected areas in (a) using the reported algorithm. (d1)–(d3). The orange and red line profiles correspond to the marks in the (b1)–(b3) and (c1)–(c3), respectively.

performance compared with the iterative phase retrieval algorithms. The improvement in imaging resolution can be quantitatively examined by comparing their phase cross sections (labeled by the red and orange lines), as shown in Figs. 4(d1)–4(d3). Obviously, the closely spaced sub-cellar features can be clearly resolved in the reconstruction of the proposed approach, while they cannot be readily observed with the traditional G-S iteration method.

Next, we verify the dynamic phase imaging ability of the proposed approach for slow-moving objects, such as live cells. Experiments were carried out on HeLa cells cultured on Petri dishes in 10% fetal bovine serum and 90% Dulbecco's modified eagle medium. Due to the relatively low speed of motion, the cells were approximately static within the spatio-temporal window of the reconstruction algorithm, and the difference between two consecutive images mainly results from the sub-pixel shift induced by the active micro-scanning. In Visualization 1, we show the full FOV dynamic SR phase reconstruction of HeLa over 5 min, with two zoom-in regions showing details about subcellular dynamics. Since the phase reconstruction result is updated for every individual raw frame, a dynamic imaging speed of 2 frames per second can be achieved, allowing for both recovering SR quantitative phase videos and following the temporal variations of the cells. It should be mentioned that the imaging speed can be further improved by simply using faster micro-servos and a camera with a higher frame rate.

Finally, we demonstrate the potentials of the proposed method for time-lapse imaging and sub-cellular feature tracking in Fig. 5. The first row of Fig. 5 gives the recovered phase distributions of HeLa cells over 30 min. In the second line, the 2D line profiles across the section marked by the red line in Fig. 5 show the migration process of two point-like structures inside the cell. At first, the selected structures were clearly separated; then their demarcation lines became blurred gradually. To observe the temporal trajectory of the single particle inside the cell, we tracked another point-like structure marked by the green dot (pointed by the white arrow), as shown in Fig. 5. The 2D projection of the trajectory is slightly zigzagged, with the total migration distance over 7 μm during the whole course of 30 min. Note that the background artifacts in the reconstruction result are mainly caused by the incomplete removal of the twin image and unwanted interference fringes arising from the cover glass of the image sensor.

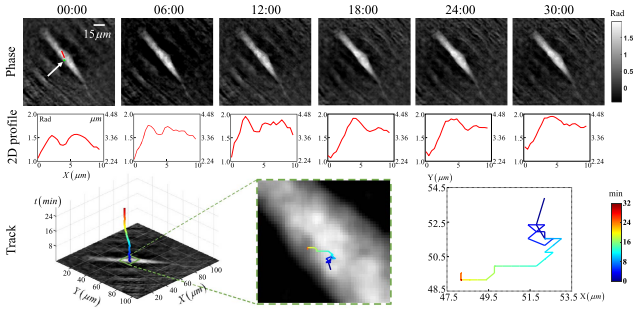


**Fig. 5.** Dynamic phase imaging of HeLa cells in culture. The first row shows the phase distributions of HeLa cells in different periods. The second row shows the corresponding cell thickness cross sections labeled by the red line. The third row shows the dynamic trajectories of the particle marked by the green dot.

In conclusion, we present a low-cost active micro-scanning-based lensfree imaging platform and associated phase retrieval algorithm to achieve dynamic SR phase imaging. This system's design includes two rotatable parallel plates within the beam path, permitting controllable source micro-scanning and sub-pixel shifts of holograms on the sensor surface. By exploiting such sub-pixel shifts between consecutive image frames in a recursive manner, both the spatial resolution and the phase imaging quality can be significantly enhanced based on a unified computational framework for phase retrieval and pixel SR. To demonstrate the resolution and dynamic imaging capabilities of the lensfree microscope, we imaged a phase resolution target and unstained HeLa cells. The presented approach extends the capability of lensfree microscopy for high-resolution QPI of dynamic samples, providing a simple and cost-effective platform to monitor large cell colonies over an extended period of time, and performs label-free cell analysis and feature tracking.

**Funding.** National Natural Science Fund of China (111574152, 61505081, 61722506); Final Assembly "13th Five-Year Plan" Advanced Research Project of China (30102070102); National Defense Science and Technology Foundation of China (0106173); Outstanding Youth Foundation of Jiangsu Province of China (BK20170034); The Key Research and Development Program of Jiangsu Province, China (BE2017162); "Six Talent Peaks" project of Jiangsu Province, China (2015-DZXX-009); "333 Engineering" Research Project of Jiangsu Province, China (BRA2016407); Fundamental Research Funds for the Central Universities (30916011322, 30917011204); Equipment Advanced Research Fund of China (61404150202).

## REFERENCES

1. G. Zheng, S. A. Lee, Y. Antebi, M. B. Elowitz, and C. Yang, Proc. Natl. Acad. Sci. USA **108**, 16889 (2011).
2. A. Ozcan and E. McLeod, Annu. Rev. Biomed. Eng. **18**, 77 (2016).
3. J. Zhang, J. Sun, Q. Chen, J. Li, and C. Zuo, Sci. Rep. **7**, 11777 (2017).
4. W. Bishara, T.-W. Su, A. F. Coskun, and A. Ozcan, Opt. Express **18**, 11181 (2010).
5. W. Luo, Y. Zhang, Z. Göröcs, A. Feizi, and A. Ozcan, Sci. Rep. **6**, 22738 (2016).
6. S. C. Park, M. K. Park, and M. G. Kang, IEEE Signal Process. Mag. **20** (3), 21 (2003).
7. W. Bishara, U. Sikora, O. Mudanyali, T.-W. Su, O. Yaglidere, S. Luckhart, and A. Ozcan, Lab Chip **11**, 1276 (2011).
8. W. Luo, Y. Zhang, A. Feizi, Z. Göröcs, and A. Ozcan, Light Sci. Appl. **5**, e16060 (2016).
9. W. Luo, A. Greenbaum, Y. Zhang, and A. Ozcan, Light Sci. Appl. **4**, e261 (2015).
10. A. Barty, K. A. Nugent, D. Paganin, and A. Roberts, Opt. Lett. **23**, 817 (1998).
11. G. Popescu, *Quantitative Phase Imaging of Cells and Tissues* (McGraw Hill, 2011).
12. F. Zernike, Physica **9**, 686 (1942).
13. R. D. Allen, G. B. David, and G. Nomarski, Z. Wiss. Mikrosk. Mikrosk. Tech. **69**, 193 (1969).
14. D. Ryu, Z. Wang, K. He, G. Zheng, R. Horstmeyer, and O. Cossairt, Biomed. Opt. Express **8**, 1981 (2017).
15. M. Guizar-Sicairos, S. T. Thurman, and J. R. Fienup, Opt. Lett. **33**, 156 (2008).
16. C. Zuo, Q. Chen, and A. Asundi, Opt. Express **22**, 9220 (2014).
17. G. Yang, B. Dong, B. Gu, J. Zhuang, and O. K. Ersoy, Appl. Opt. **33**, 209 (1994).
18. E. D. Barone-Nugent, A. Barty, and K. A. Nugent, J. Microsc. **206**, 194 (2002).